Journal of Applied Electrochemistry (2005) 35:521–528
DOI 10.1007/s10800-004-3995-8

Carbon deposition and alkali poisoning at each point of the reforming catalysts in DIR-MCFC

JUNG-HO WEE and KWAN-YOUNG LEE*
Department of Chemical and Biological Engineering, Korea University, Seoul 136-701, Korea
*(*author for correspondence, fax: 82-2-926-6102, e-mail: kylee@korea.ac.kr)*

Received 25 May 2004; accepted 7 September 2004

Key words: carbon deposition, direct internal reforming, molten carbonate fuel cell, poisoning of alkalis, reforming catalyst

Abstract

The extent of local carbon deposition and alkali poisoning of the reforming catalysts in a unit cell (5×5 cm) of a direct internal reforming molten carbonate fuel cell was examined. The catalysts in the catalyst bed were sampled from 25 points individually after the unit cell had been operated for both 24 and 100 h, and the amount of carbon, alkali poisoning were then analyzed. There was little difference in the amount of carbon deposition and alkali poisoning with respect to the direction of the cathode gas. They were only dependent on the direction of the anode gas. After 24 h, the amount of carbon deposited on the catalysts loaded in the front region, and the extent of alkali poisoning in the catalysts loaded in the rear region were relatively higher than those of any other regions. After 100 h, the amount of carbon deposition in the catalysts loaded in the front region was still the highest and the amount of alkali poisoning increased rapidly. Meanwhile, relatively low carbon deposition rate and the small increase in alkali poisoning were observed in the catalysts loaded in the rear region. Therefore, the rate of alkali poisoning of the catalyst in the rear region was much slower than those in any other region. These results for catalyst poisoning were explained by a simulation of the unit cell, which was performed to determine the temperature profiles and the extent of the reaction at each point of the unit cell. The simulation showed that the catalysts in the front region treated 90 mol% of the initial methane flow, and the temperature was the lowest at this region. Therefore, the catalysts in this region had the highest level of carbon deposition and the rate of alkali poisoning was faster than that of the catalysts in the other regions. This simulation also explained the reasons for the relatively low level of carbon deposition in the rear region, as well as the relatively high rate of alkali poisoning from the start and the low rate of alkali poisoning in the rear region.

1. Introduction

A direct internal reforming molten carbonate fuel cell (DIR-MCFC) produces hydrogen directly and continuously by the steam reforming of methane in a catalytic bed on top of an anodic electrode. This also uses the heat released by the electrochemical reaction as a source of heat essential for the endothermic catalytic reforming reaction. Therefore, DIR-MCFC is an attractive device in view of energy and fuel efficiency. However, there are several disadvantages. One of these is the fall in the cell performance as a result of poisoning of the reforming catalysts. This is the result of the reforming and electrochemical reactions not being uniformly distributed over the entire catalytic bed and the unstable temperature variations of the cell. Therefore, the reforming catalysts are attacked by carbon deposition and alkali poisoning during operation. In particular, the key problems of catalyst poisoning due to potassium and lithium vaporization from the electrolyte via the anode to the catalytic bed needs to be solved in order for more advanced DIR-MCFC to be produced. Several methods, including the preparation of alkali-poisoning-resistant catalysts and the change in the structures of the cell body, have been developed to improve these catalytic problems of DIR-MCFC [1–5]. In addition, several studies have elucidated the mechanisms of carbon deposition and alkali poisoning on steam reforming catalysts [1–5]. However, there have been no studies on carbon deposition and alkali poisoning on catalysts at different points in the cell during the DIR-MCFC unit cell operation.

In order to examine the extent of catalyst poisoning at each point in a the cell, experiments at a steady state were performed for 24 and 100 h with a unit cell size of 5×5 cm, where anode and cathode gases flowed perpendicularly to each other. Catalysts from 25 divided normal squares (1×1 cm) of the cell were sampled and analyzed for carbon, potassium and lithium. The temperature distributions, the reforming reaction rate, the electrochemical reaction rate and the amount of water accumulated at each point of the cell were acquired from

the simulation (J.H. Wee and K.Y. Lee, submitted) to determine the optimum operating condition of DIR-MCFC. The simulation results could explain the reason for the extent of the poisoning phenomena on reforming catalysts.

This paper is intended to provide an insight in solving catalytic problems in a DIR-MCFC with more quantitative information about carbon deposition and the extent of alkali poisoning on reforming catalysts during cell operation.

2. Theory

2.1. *Reaction at DIR-MCFC*

In the DIR-MCFC system, methane, which is the main component of natural gas, is fed to a catalyst bed, which is in direct contact with the anode on top. Hydrogen, which is the cell fuel, is produced by steam–methane reforming, as shown in Equation 1, and by a water gas shift reaction, as shown in Equation 2. The hydrogen produced by these catalytic reactions is consumed at the anode in the electrochemical reaction, as shown in Equation 3. Equation 4 shows the reaction occurring at the cathode. Therefore, the overall reaction for DIR-MCFC can be expressed as Equation 5.

The catalysts for the reforming reaction can be poisoned and deactivated by both carbon and the electrolyte during the cell operation. Carbon deposition due to an unstable temperature distribution including the well known Boudouard reaction, Equation 6, and alkali poisoning, as a result of vaporization from the electrolyte, deteriorate the cell performance. Carbon deposition can be controlled slightly by adjusting the operating conditions. However, the attack of the reforming catalysts is the result of alkali vapor diffusing from the electrolyte through the pores and the spaces formed by creep of the anode electrode, which adversely affects the cell performance. Alkali poisoning can occur in several different ways such as pore filling, pore plugging, and coating of the nickel catalyst surface, which decreases the specific activity and enhances the sintering of the nickel crystallites [5].

$$CH_4 + H_2O \Leftrightarrow 3H_2 + CO \quad (1)$$

$$CO + H_2O \Leftrightarrow H_2 + CO_2 \quad (2)$$

$$H_2 + CO_3^{2-} \Leftrightarrow H_2O + CO_2 + 2e^- \quad (3)$$

$$1/2O_2 + CO_2 + 2e^- \Leftrightarrow CO_3^{2-} \quad (4)$$

$$H_2 + 1/2O_2 + CO_2(\text{cathode}) \Leftrightarrow H_2O + CO_2(\text{anode}) \quad (5)$$

$$2CO \Leftrightarrow C + CO_2 \quad (6)$$

2.2. *Reforming catalysts in the DIR-MCFC*

Several studies aimed at eliminating alkali diffusion and preventing poisoning of the reforming catalysts have been performed [4, 5, J. H. Wee and K.Y. Lee, submitted, 6–17]. These can be classified into three basic categories. The first attempt, beginning from the mid-1980s, was the preparation and development of alkali-resistant reforming catalysts. The Ni support was substituted with alkali-resistant MgO [6–12], Al_2O_3 [5], Cr_2O_3, SiO_2, γ-$LiAlO_2$, α-$LiAlO_2$ and YSZ [12–13]. Metal oxides were added [14] and promoters such as Ru or Rh were used [4]. The Ni support was also doped with Al, La and Mg [4, 5]. The second series of attempts, which began in the middle 1990s, modified the structure of the anodic chamber. A protective shield was inserted between the anode and the catalysts to protect the catalysts from alkali attack. This shield which was pervious only to hydrogen and not to alkali was made of a porous plate, foil, ceramic and membrane [15–18]. A third attempt began recently in the 2000s, and was directed at finding new optimum operating conditions of the DIR-MCFC in order to reduce alkali poisoning as much as possible. The new operating conditions include changes in the loading positions of the catalysts, the steam to carbon ratio and maintaining uniform gas conditions [19].

2.3. *Carbon deposition of reforming catalysts in DIR-MCFC*

There have been several studies on carbon deposition in reforming catalysts. There are three types of carbon formation in the catalytic reforming of hydrocarbons via different routes [5]. The formed carbon may cause the breakdown of the catalyst particles and the encapsulation of the active sites of the catalysts. Many methods to avoid carbon deposition were presented. These suggest that precise controls of the reforming temperature and the steam to carbon ratio are the key factors in solving the problem [7, 8]. In DIR-MCFC, an operating temperature of 650 °C and a steam to carbon ratio >2.0 are theoretically sufficient to avoid carbon deposition. However, a small amount carbon deposition is unavoidable due to the presence of cold spots, which are formed when the endothermic steam–methane reforming reaction is carried out [20].

2.4. *Alkali poisoning of reforming catalysts in DIR-MCFC*

One of the key issues in DIR-MCFC is alkali poisoning of the reforming catalysts. There are many theories for

the effects of alkali addition and adsorption on reforming catalysts [4]. Kinetic theory suggests that potassium, which is generally used as a promoter in nickel based reforming catalysts to suppress carbon formation [21], reduces the order of the reforming reaction rate. However, it leaves the activation energy unchanged [22, 23]. According to quantum dynamics, the adsorption of an alkali atom to a nickel atom causes variations in the electronic characteristic value of the nickel atom [24]. In medium theory, adsorption of an alkali would accelerate the adsorption of steam to the nickel surface but has no influence on either the methane adsorption rate or the activation energy [25]. Consequently, these theories do not provide a clear explanation for the precise function and effect of alkali adsorption on nickel catalysts. It is very difficult to explain the mutual relationship between the alkali and nickel electronically and chemically. In addition, there is insufficient evidence to support it [24]. Alkali poisoning of catalysts can only be explained by the reconstruction or faceting of the nickel active site with the alkali [24].

3. Experimental

3.1. *Unit cell operation of DIR-MCFC*

When the unit cell was under operation, anode gases and cathode gases flowed perpendicularly to each other. The steam to carbon ratio was 2.5, and the operating voltage and average current density were 0.70 V and 140 mA cm^{-2}, respectively. The disassembled unit cell for this study is shown in Figure 1.

Figure 2 shows a schematic of the experimental apparatus used in this study.

Table 1 shows the optimum conditions and the other characteristics of the unit cell operation, which were acquired from previous experimental data (J.H. Wee and K.Y. Lee, submitted). This table includes the experimental data such as the characteristics of the components of the unit cell, the reforming catalysts, anode, cathode and electrolyte as well as the operating conditions of the experiments such as the current density, utilization, total pressure and operating voltage. Table 2 provides details of the catalyst used.

Using these conditions, the experiments were carried out for 24 and 100 h after a steady state had been reached.

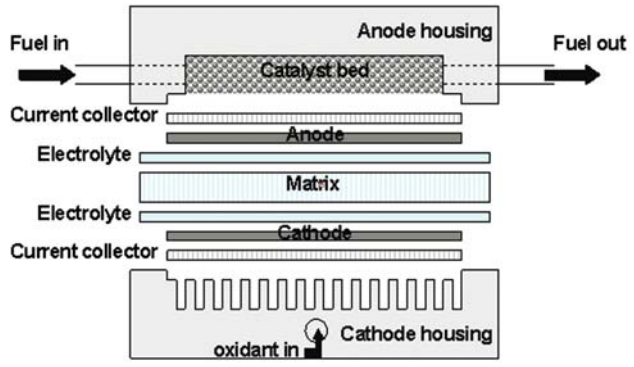

Fig. 1. Configuration of the disassembled DIR-MCFC.

3.2. *Analysis of carbon, potassium and lithium in reforming catalysts*

The unit cell was carefully disassembled after operating at steady state for 24 and 100 h. The catalysts loaded in the catalytic bed in the anode chamber were then divided into 25 regular squares and labeled with x, y coordinates, as shown in Figure 3. The x-axis denotes the direction of the anode gas flow, and y-axis denotes the direction of the cathode gases. These labeled catalysts were sampled, and the amount of carbon, potassium and lithium was analyzed. The variation in the physical surface area and hydrogen chemical adsorption of the poisoned catalysts were investigated by BET (Micrometrics, ASAP 2010). A carbon analyzer (Shimadzu, TOC-5000) and ICP-AES (Jobin yvon emission instrument, JY138 ULTRACE) were used to determine the amount of carbon, potassium and lithium deposited.

4. The simulation for performance of DIR-MCFC

In order to examine the relationship between catalyst poisoning and the reactions within the unit cell, simulations, which predicted the rates of the steam-methane reforming reaction, the electrochemical reaction and the temperature distribution at each point of a unit cell, were carried out. The simulations were based on the material balance for each component gas and also on the equilibrium equations for the reaction. Equations for the local current density and the energy balance were also used. These four balances and equations used to search for the rate of the reactions, and the temperature distribution at an arbitrary square point (x, y) of the fuel cell were mutually coupled. The solutions were acquired using a standard matrix technique, and the iteration method was performed using mutual correction and convergence to a certain value. We could validate our mathematical model by comparing the exit gases compositions calculated by the model with those of experimental results. More information about these simulation results are reported elsewhere (J.H. Wee and K.Y. Lee, submitted).

5. Results and discussion

5.1. *The poisoning of reforming catalysts predicted by simulation results*

Figure 4 shows the simulation results such as the extent of the steam–methane reforming reaction, the

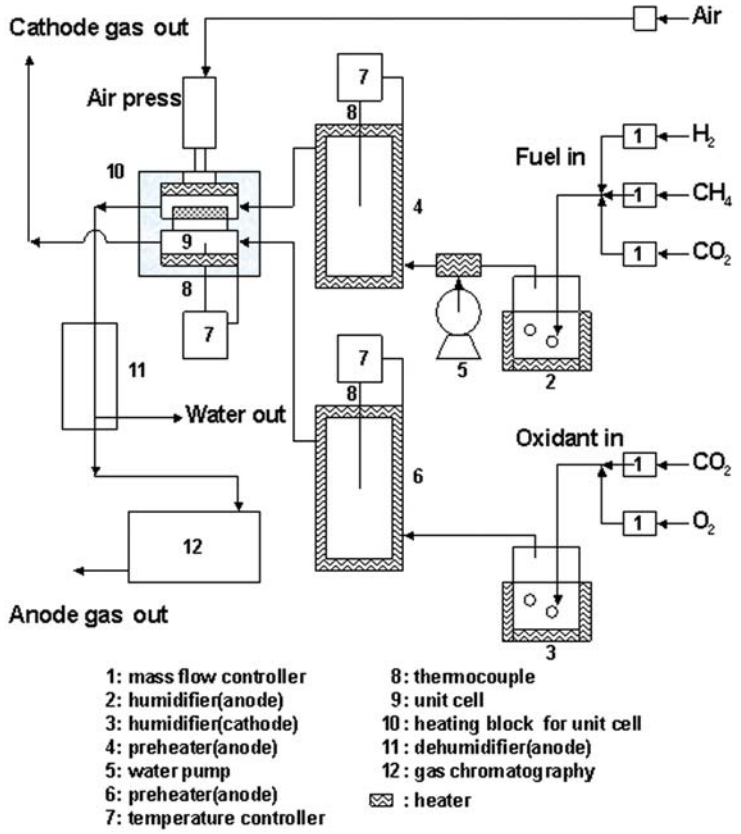

Fig. 2. Schematic diagram of the experimental apparatus for performance of the DIR-MCFC.

Table 1. Operating conditions and the other characteristics of the unit cell operation

Unit cell and operating conditions	Value and characteristics
Unit cell	
Housing	
Size (width × length; cm × cm)	7 × 7
Material	SUS-316
Catalysts	
Weight of loaded (g)	6.25
Characteristics	Referred to Table 2
Anode electrode	
Size (width × length; cm × cm)	5 × 5
Material	Ni
Feed rate of methane (mol h^{-1})	0.0402
Temperature of methane (°C)	650
Steam to carbon ratio	2.5
Cathode electrode	
Size (width × length; cm × cm)	5 × 5
Material	NiO
Feed rate of carbon dioxide (mol h^{-1})	0.1608
Feed rate of oxygen (mol h^{-1})	0.0804
Electrolyte	
Matrix	γ-$LiAlO_2$
Li (Li_2CO_3)/K (K_2CO_3) mole ratio	62/38
Current density (mA cm^{-2})	140
Operation voltage (V)	0.7
Total pressure (atm)	1
Utilization (%)	40

electrochemical reaction in the anode for hydrogen and the amount of accumulated water as a result of the reaction at each of the 25 points.

Figure 5 shows the temperature distributions of the anode gas predicted using the simulation.

These two figures show that there are large differences in both the extent of the reforming reaction and the temperature distribution at each point on the anode electrode. These results highlight the roles of reforming catalysts and can predict the poisoning of the reforming

Table 2. The properties of the fresh reforming catalysts

Properties (unit)	Characteristic and value
Average pore radius (Å)	113.40
Bulk density (g cm^{-3})	1.85×10^{-3}
Composition (wt %)	Ni: 28.74, Mg: 33.38, K: 0.17
Ni dispersion (%)	2.10
Ni particle size (nm)	52.00
Porosity (%)	13.14
Shape	Cylindrical pellet
Size	
Diameter (mm)	1.24
Length (mm)	1.80
Specific BET area	
At 25 °C (m^2 g^{-1})	53.88
At 650 °C (m^2 g^{-1})	48.45
Specific pore volume (ml g^{-1})	0.31

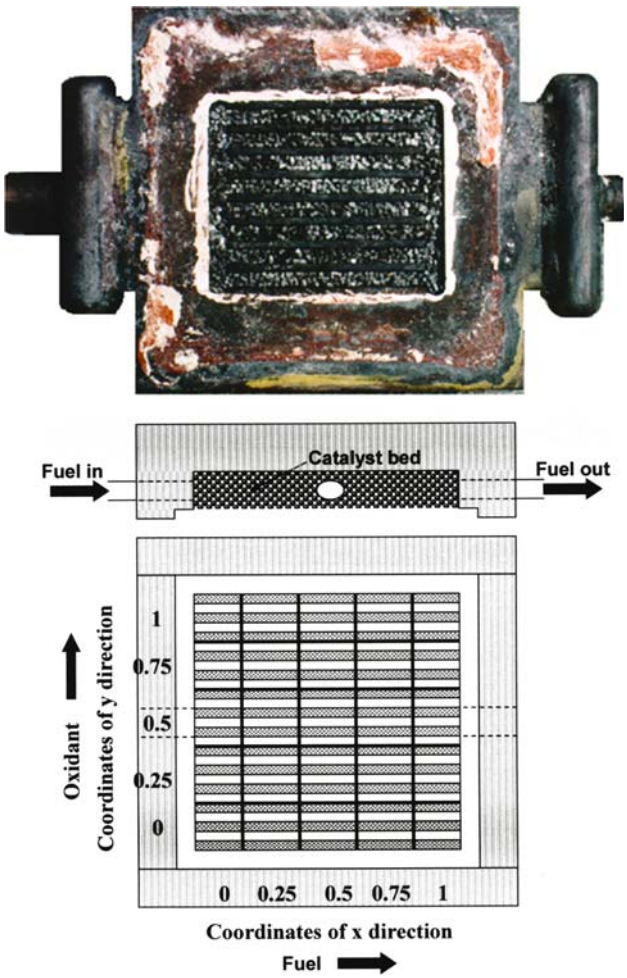

Fig. 3. A photograph and its corresponding overview of the reforming catalysts loaded in the anodic catalysts bed and divided into 25 coordinated normal squares for analysis.

catalysts at each point. First of all, in the front region of the unit cell, there was rapid heat transfer between these 2 endo–exothermic reactions because 90 mol% of the feeding methane had reformed to hydrogen and an electrochemical reaction had occurred. Therefore, the temperature in this region was the lowest, as shown in Figure 5. The reforming catalysts loaded in this area received more thermal impact and were damaged predominantly by carbon deposition and alkali poisoning. This trend in catalyst damage was strengthened as the operating time progressed.

On the other hand, the catalysts loaded in the rear region of the unit cell made a small contribution to the reforming process, and the temperature of this region was 30 °C higher than that of the front region. The high temperature accelerated the vaporization of the two alkalis. The water produced by the reaction accumulated in the rear region, which suppressed carbon deposition and increased the solubility of the alkali.

5.2. *The variation in the total surface area and the number of active sites on the reforming catalysts at each point*

Figure 3 shows an overview photograph. Each location was assigned one of the 25 normal divided squares of the catalyst bed. The photograph shows the catalysts and the bed prior to sampling. The extent of catalyst poisoning was found to be dependent on the direction of the anode gas, but was largely unaffected by the direction of the cathode. Figure 6 shows the changes in the surface area of the catalysts according to the sintering temperature. The surface area of the fresh catalyst was 53.9 $cm^2\ g^{-1}$. However, the surface area decreased to 48.5 $cm^2\ g^{-1}$ after the fresh catalysts were maintained at 650 °C for 100 h. Therefore, there was a 10% reduction in the surface area of the catalysts as a

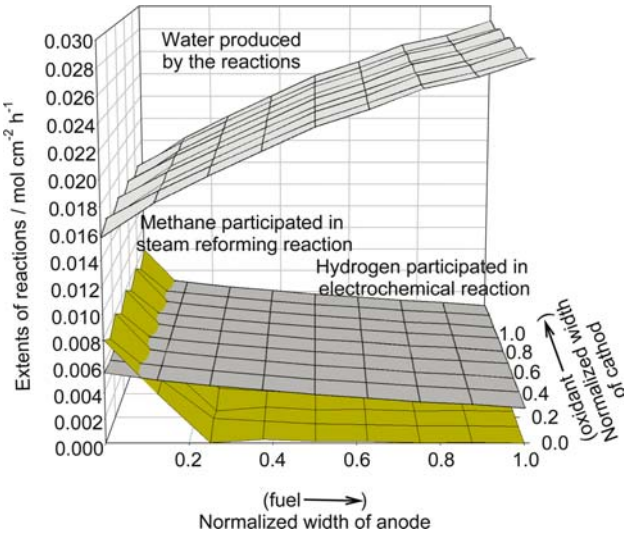

Fig. 4. Local extents of the steam-methane reforming reaction for methane, the electrochemical reaction for hydrogen and the amounts of water produced by the reaction at the 25 points of the anodic part of the unit cell (J.H. Wee and K.Y. Lee, submitted).

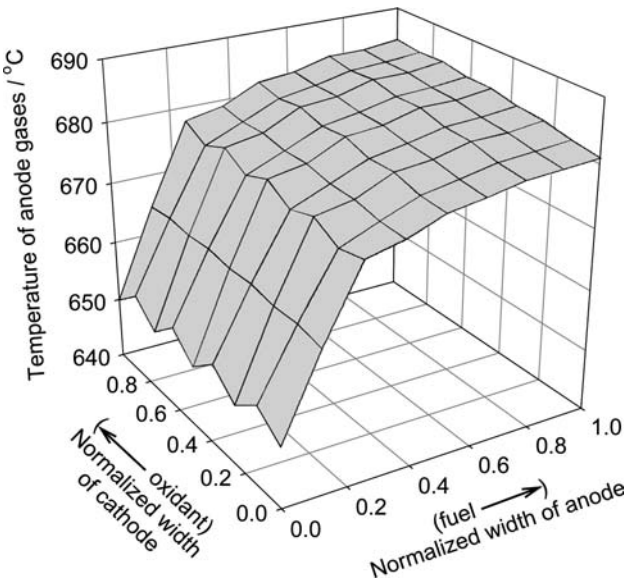

Fig. 5. Temperature distributions of the anode gas at 25 points of anodic part of the unit cell (J.H. Wee and K.Y. Lee, submitted).

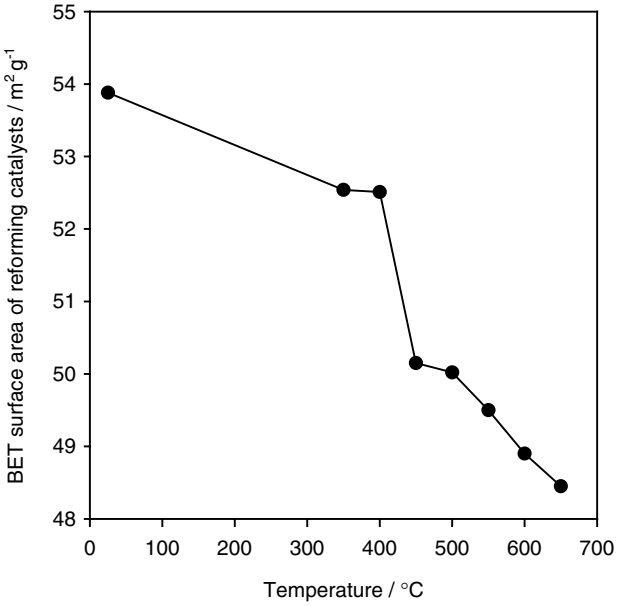

Fig. 6. Changes in the BET surface area of the fresh reforming catalysts as a function of the temperature.

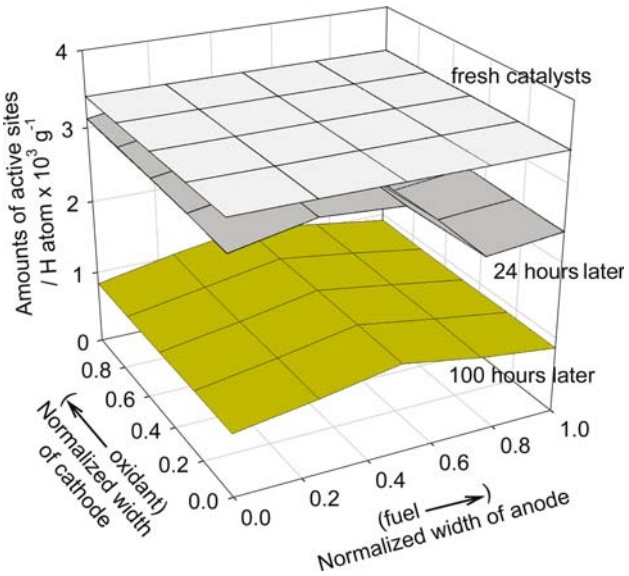

Fig. 8. Changes in the amount of active sites of the catalysts at the 25 points according to the operating time.

result of sintering, which was found to occur between 400 and 450 °C.

After operating the unit cell for 24 h, the surface area decreased by an average of 4.3 $cm^2\ g^{-1}$ and was not significantly different at each point, as shown in Figure 7.

After 100 h of operation, the BET surface area of catalysts in the front region was the lowest at 33.2 $cm^2\ g^{-1}$. The BET surface area increased steadily towards the middle region (43.3 $m^2\ g^{-1}$) and decreased towards the end of the cell (38.5 $cm^2\ g^{-1}$). This result is similar to the trend in the changes in the number of active sites measured by hydrogen chemisorption, as shown in Figure 8. Although Figures 7 and 8 show similar trends, the decrease in the number of active sites as a function of the operating time was relatively faster than the reduction in the BET surface area. This suggests that alkali poisoning of the catalyst increases with increasing operating time. It appears that the catalysts loaded in the front and rear regions were damaged more than those in the middle region.

5.3. *Carbon deposition and alkali poisoning of the reforming catalysts at each point*

Figure 9 shows the amount of carbon deposition and alkali at each point of catalysts after 24 h of operation. The amount of carbon deposition at point (0, 0.5) was 1.85 wt %, which was the highest, and decreased to

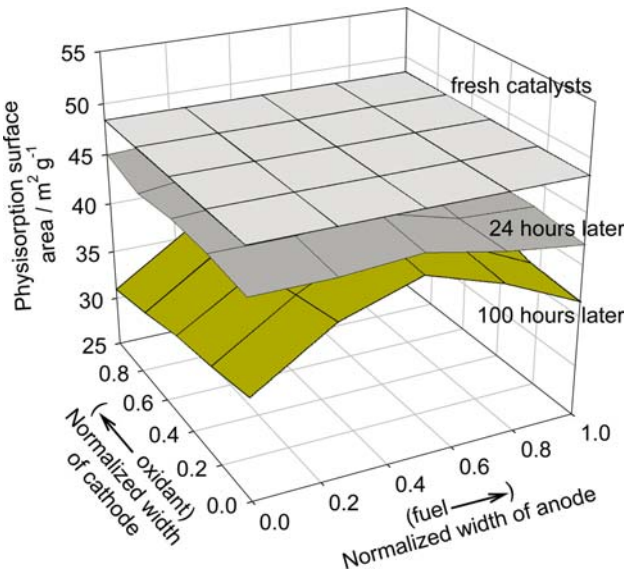

Fig. 7. Changes in the BET surface area of the catalysts at the 25 points according to the operating time.

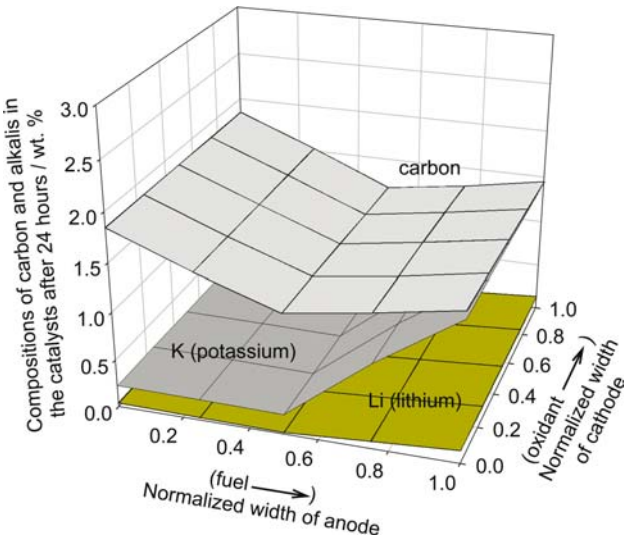

Fig. 9. Compositions of the carbon deposits and alkali poisons in the catalysts at the 25 points after 24 h operating time.

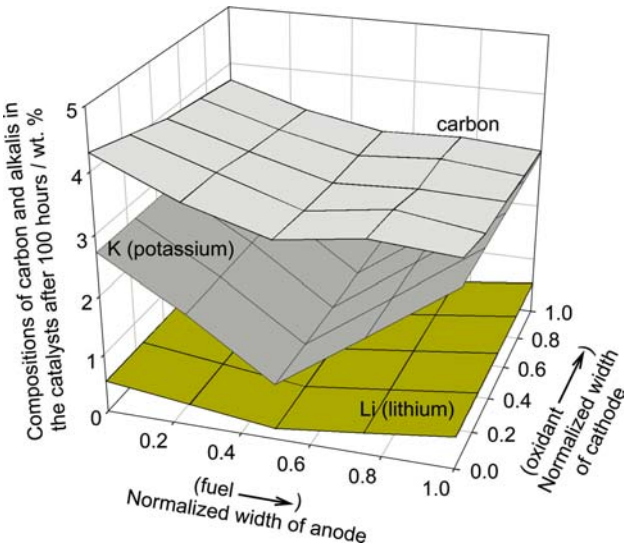

Fig. 10. Compositions of the carbon deposits and alkali poisons in the catalysts from the 25 points after 100 h of operation.

1.53 wt % at point (0.25, 0.5). The center point (0.5, 0.5) showed the lowest value of 1.22 wt %. From point (0.5, 0.5), carbon deposition increased slightly to 1.35 wt % at point (0.75, 0.5), and to 1.49 wt % at the end point (1, 0.5). The amount of alkali poisoning varied from the front to the middle region. The potassium level was the same at 0.22 wt % from point (0, 0.5) to point (0.5, 0.5) and the lithium level was 0.04 and 0.02 wt % at those points, respectively. However, the catalysts loaded from the center point to the end point were poisoned more rapidly. The potassium level at (0.75, 0.5) and (1.0, 0.5) was 0.88 and 1.45 wt%, and lithium level was 0.08 and 0.14 wt%, respectively.

Figure 10 shows the amount of carbon deposition and alkali poisoning at each point of the catalysts after 100 h of operation. The amount of carbon deposition was the highest as 4.3 wt% at point (0, 0). This can be explained by the simulation results of the lowest temperature, which showed the highest rate of the steam–methane reforming reaction, and relatively low water composition at this point. In addition, the extent of potassium and lithium poisoning was high at this point. This was attributed to the electrochemical reaction rate at this point being very high, resulting in a large amount of alkali moving into this region. On the other hand, the level of carbon deposition was lower for the catalysts in the rear region than that in any other region for the following reasons: high temperatures, low extent of the steam–methane reforming reaction, and sufficient water accumulated. The amount of alkali in the rear region was high, which was similar to that in the front region.

Figure 11 shows the extent of alkali poisoning at the front and rear region. The rate of poisoning at the front region was higher than that of the rear region, particularly in the case of potassium poisoning. This different rate of potassium poisoning can be explained as follows: alkali poisoning at the front region during operation of the fuel cell is mainly due to an electrochemical reaction, and the poisoning that occurs in the rear region is caused by vaporization as a result of the relatively high temperature, which is accelerated by water accumulation.

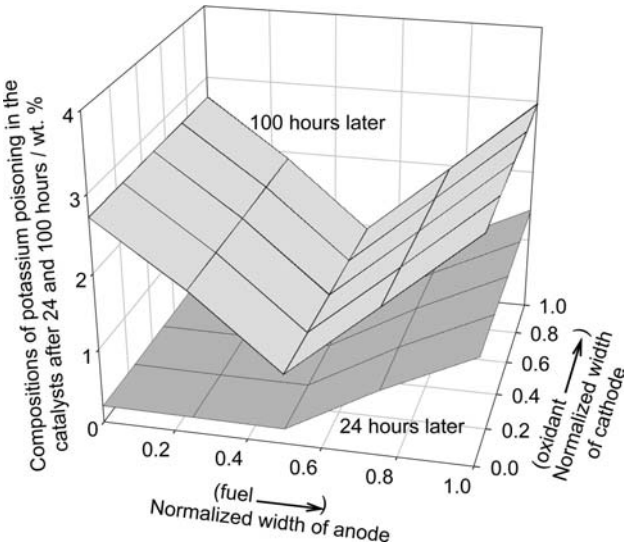

Fig. 11. Rate of potassium poisoning in the catalysts at the 25 points.

6. Conclusions

The extent of poisoning of the reforming catalysts including carbon deposition, were different at each position of the catalysts loaded in the DIR-MCFC. This was explained by the simulation results regarding the temperature distribution, as well as the extent of the steam-methane reforming reaction and the electrochemical reaction. The results are intended to provide useful information for development of better reforming catalysts, design and operating conditions of the DIR-MCFC.

Acknowledgement

The authors appreciate the support by research grants from the Korea Science and Engineering Foundation (KOSEF) through the Applied Rheology Center (ARC) at Korea University.

References

1. A.M. Gadalla and B. Bower, *Chem. Eng. Sci.* **43** (1988) 3049.
2. S. Cavallaro, S. Freni, R. Cannistraci, M. Aquino and N. Giordano, *Int. J. Hydrogen Energy.* **17** (1992) 181.
3. A. Takano, T. Tagawa and S. Goto, *J. Chem. Eng. Jpn.* **27** (1994) 727.
4. J.R. Rostrup-Nielsen and L.J. Christiansen, *Appl. Catal. A: Gen.* **126** (1995) 381.
5. R.J. Berger, E.B.M. Doesburg, J.G. van Ommen and J.R.H. Ross, *Appl. Catal. A: Gen.* **143** (1996) 343.
6. K. Kishida, *Ber. Bunsen, Phys. Chem. Chem. Phys.* **94** (1990) 941.
7. R.J. Selman, *Energy (Oxford)* **11** (1986) 153.

8. K. Kishida, E. Nishayama, M. Matsumura, T. Tanaka, S. Kaneko, Y. Mori and S. Nakagawa, 'Extended Abstracts of the International Seminar on Fuel Cell Technology and Applications', (Scheveningen, The Netherlands, 26–29 October, 1987) pp 40.
9. N. Giordano, F. Frustreri, P. Tsiakaras, A. Mezzapica and A. Parmaliana, *in* 'Abstracts of the Fuel Cell Seminar', (Tuscon, USA, 26–29 October, 1986) p. 230.
10. R.J. Berger, E.G.M. Doesburg, J.G. van Ommen and J.R.H. Foss, *Catalysis Sci. Technol.* **1** (1991) 455.
11. V.A. Sobanyin, I.I. Bodrova, E.Y. Titova, O.V. Bazhan, V.D. Belyaev and N.N. Bodrov, *React. Kinet. Catal. Lett.* **39** (1989) 443.
12. M. Tarjanyi, L. Paetch, R. Bernard and H. Ghezel-Ayagh, Proceedings International Seminar on Fuel Cells, Tuscon, USA, 19–22 May 1985 p. 177.
13. T. Takeguchi, Y. Kani, T. Yano, R. Kikuchi, K. Eguchi, K. Tsujimoto, Y. Uchida, A. Ueno, K. Omoshiki and M. Aizawa, *J. Power Sources* **112** (2002) 588.
14. M. Ito, T. Tagawa and S. Goto, *Appl. Catal. A: Gen.* **184** (1999) 73.
15. E. Passalacqua, S. Freni, F. Barone and A. Patti, *Mater. Lett.* **29** (1996) 177.
16. E. Passalacqua, S. Freni and F. Barone, *Mat. Lett.* **34** (1998) 257.
17. T. Yamaguchi, M. Ibe, B.N. Nair and S. Nakao, *J. Electrochem. Soc.* **149** (2002) 1448.
18. M. Keijzer, K. Hemmes, J.H.W. De Wit and J. Schoonman, *J. Appl. Electrochem.* **30** (2000) 1421.
19. K. Sugiura, M. Daimon and K. Tanimoto, *J. Power Sources* **118** (2003) 228.
20. T. Mori, K. Higashiyama and S. Yoshioka, *J. Electrochem. Soc.* **136** (1989) 2230.
21. S. Carvallaro, E. Passalacqua, G. Maggio and A. Patti, 'Program and Abstracts, Fuel Cell Seminar' (Courtesy Associates Inc.', Washington, DC 1996) p. 442.
22. J.R. Rostrup-Nielsen, 'Catalytic Steam Reforming, Catalysis, Science and Technology', *in* J.R. Anderson and M. Boudart (Eds), Vol. 5, (Springer-Verlag, New York, 1984) p. 1.
23. L.G. Marianowskin and G. Vogel, EP 0257398 A2 (1987).
24. A.R. West, 'Solid State Chemistry and Its Applications' (John Wiley & sons, 1989) p. 742.
25. D.A. Spagnolo, L.J. Cornett and K.T. Chuang, *Int. J. Hydrogen Energy* **17** (1992) 839.